PalMod – Paleo Modeling

From the Last Interglacial to the Anthropocene –
Modeling a Complete Glacial Cycle

Principal Investigators: Mojib Latif[1], Tatiana Ilynia[2], Martin Claussen[2], Michael Schulz[3]
Program Coordination: Tim Brücher[1] (tbruecher@geomar.de)

(1) GEOMAR, Kiel; (2) MPI-M, Hamburg; (3) MARUM, Bremen

PalMod is grateful for the computing time granted in 2018. Each PalMod Working Group (WG) submitted its individual proposal, this report summarizes the work of all four work packages within PalMod:

WG1 (project 989) *Physical System*
WG2 (former project 1030) *Biogeochemistry*
WG3 (former project 1029) *Synthesis and Analysis of Proxy Data*
WG4 (former project 993) *Optimization of Quality and Performance*

Within 2018 we got 1.08 Mil. node hours granted. By end of October (2 months left) we used app. 70 % of the resources. Unfortunately, some resources couldn't be used due to delays in personal support or delays in model development. Please find more details in our reports.

PalMod is a BMBF-funded project focused on understanding earth system dynamics and variability during the last glacial cycle. The PalMod project has a time scale of 4 years, with a potential extension up to 10 years. The first project phase will focus on the time from the Last Glacial Maximum to the present, while the second phase will consider the entire last glacial cycle.

As the first phase of PalMod is devoted to develop earth system models and to identify and investigate feedbacks and processes necessary to successfully simulate the last deglaciation, the number different model versions (32) within PalMod is large. This is due to the fact, that PalMod follows a somehow modular approach with its key advantages to overcome unnecessary dependencies between the different working groups due to ongoing development. So, (i) everybody can start immediately with the tools on hand, (ii) there are only minor dependencies between the working groups, and (iii) the range of investigated models / coupling strategies is much larger, which is a benefit to investigate a larger model-space.

As announced last year, the number of PalMod publications is now growing. To this date, 60 publications have been made possible to PalMod funding and resources at DKRZ, further 75 publications in press / submitted through in-kind contributions to PalMod.

Each working group summarizes their scientific progress and their results independently. Please find the 4 reports with key highlights and justification for computing time or even unexpected delays and unused resources in the following sections.

Project: **989**

Project title: **Long transient simulations of the last deglaciation (last 30,000 years) and the development of lithosphere and ice sheet models in the framework of PalMod Working Group 1, Physical System**

Project lead: **Gerrit Lohmann**

Report period: **2017-01-01 to 2017-12-31**

We report on our modeling efforts on Mistral during the first 10 months of the allocation period 2018, covering proposed simulations with MPI-ESM, PISM, ISSM, VILMA, CCLM, and AWI-ESM[1].

At the KIT in the framework of regional ice sheet modelling, in 2016 and 2017 the model setup of the regional climate model COSMO-CLM was optimized for simulations of Arctic regions and, driven with ERA-Interim data on 0.7° resolution for the present-day period (1995-2015), on 0.22° resolution. In 2018 the added value of higher resolution was investigated based on 23-years simulations on 0.0625° resolution. In order to further improve the surface mass balance simulated by the model, more sensitivity studies were performed, leading to a much more realistic SMB of the Greenland ice sheet (Fig.1). A paper about these results is in preparation. In order to simulate also periods with other orbital conditions, an orbital routine was implemented into COSMO-CLM.

This model was driven for the CORDEX-Arctic region for GCM pre-industrial conditions (AWI; T31) and also for LGM climate conditions (AWI; T31) for 5 years each. Due to the low resolution of GCM data provided, a two-step-nesting was needed (0.88°; 0.22°). Additionally, for the CORDEX-Europe region the model was driven by GCM pre-industrial data (MPI; T31) and mid-Holocene (MPI; T31) climate conditions on 0.44° resolution for 30 years each.

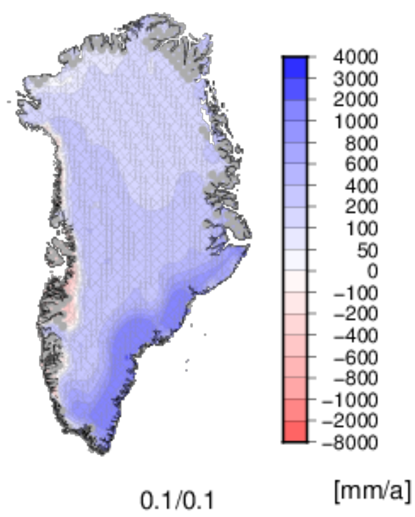

Fig. 1: Example of simulated surface mass balance obtained with the new model on 0.44°, driven with ERA-Interim data (0.7°) for 1995.

1 Note, that the AWI-CM has been renamed to AWI-ESM in the framework of contributions to CMIP6. This is in order to distinguish the version with dynamic vegetation (now called AWI-ESM) from the version without dynamic vegetation (for the latter version, the model name "AWI-CM" remains). Besides the renaming, the model did not change with respect to last year's proposal, where we still referred to the employed version, that already then considered dynamic vegetation, as "AWI-CM".

After successfully coupling the ice sheet model mPISM and the GIA model VILMA for the Northern Hemisphere during the last allocation period in 2017, MPI-Met successfully added MPI-ESM into the setup and performed the first fully coupled climate-ice-sheet simulations of the last deglaciation in an asynchronously coupled setup. Although a final tuning of the individual components and the whole setup is still ongoing – as the implementation of the new components (e.g. an energy balance model to calculate and downscale the surface mass balance (SMB) for mPISM, modules for interactive topography and river rerouting in response to ice sheet changes) took longer than planned – the simulations were essential for testing the coupling strategies and for investigating whether the interactions between ice sheets and climate within the MPI-ESM-CR-ISM setup are physically plausible. The simulations show promising results (Fig. 2). This will allow us to continue the tuning in the following allocation period and to conduct first synchronously fully coupled simulations.

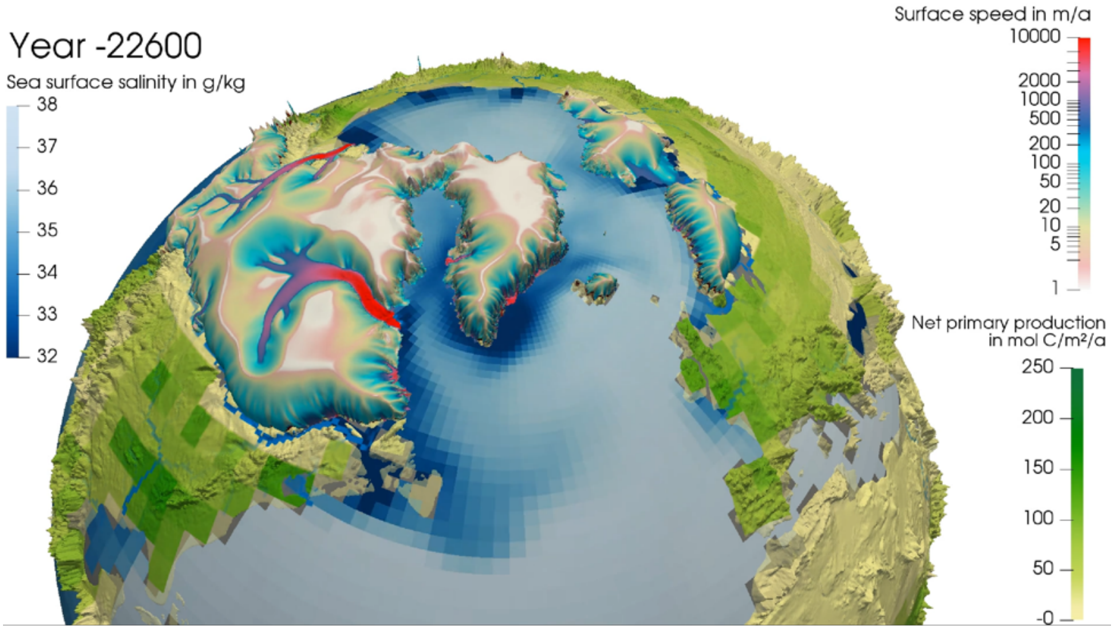

Fig. 2: Ice sheets, sea-surface salinity and primary production in a fully coupled deglacial test experiment. The colors on ice show the surface flow speed, the colors on land show the net primary production, and the colors over ocean show the sea surface salinity.

Additionally, MPI-Met has conducted simulations of the deglaciation with prescribed ice sheets and topography from different ice sheet reconstructions (ICE6G by Peltier et al. 2015 and GLAC1D by Tarasov et al., 2002, 2012). These simulations allowed us to investigate the climate's response to changes in the ice sheets. Specifically, MPI-Met investigated the response of the Atlantic Meridional Overturning Circulation (AMOC) to the freshwater input from retreating ice sheets during the deglaciation. The response differs significantly depending on the used reconstruction (Fig. 3). Interestingly, both simulations show a collapse of the AMOC during the Bølling Allerød warming (around 14 kyrs BP) due to freshwater release into the ocean from the reconstructions, which is not observed in paleo proxies. On the other hand, the AMOC collapse observed during the Younger Dyras (approx. 12 kyrs BP) is only reflected in the simulation forced with ICE6G reconstructions, due to changes in the river routing. The differences between the simulations indicate that small differences in the topography can cause significant changes in the ocean circulation. MPI-Met also analyzed changes in the SMB for these simulations and finds that the SMB over the Greenland Ice Sheet, as well as parts of the Laurentide and Fennoscandian ice sheets, is very sensitive to changes in the AMOC (not shown).

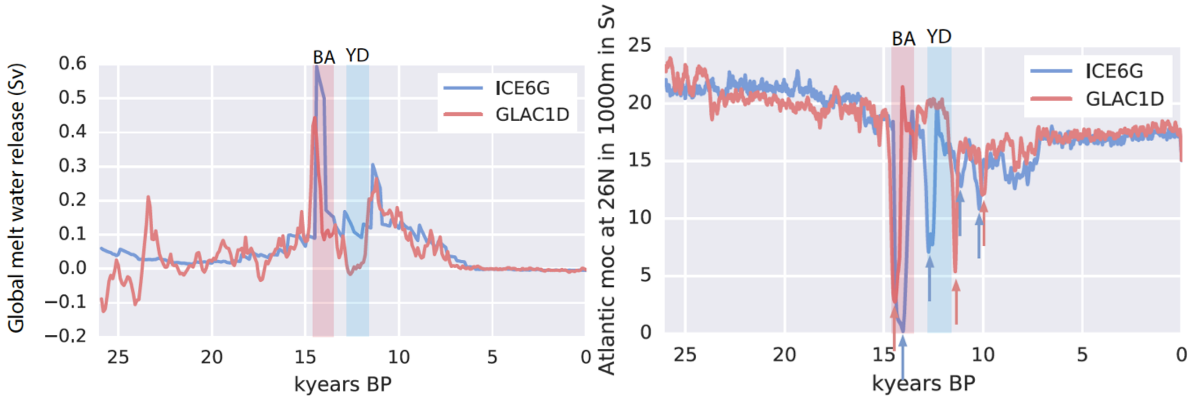

Fig. 3: Timeseries of global melt water release (left) and Atlantic Meridional Overturning Circulation (AMOC; right) from two MPI-ESM simulations with prescribed topography and fresh water release from ICE6G and GLAC1D ice sheet reconstructions. The simulation period comprises the last deglaciation (21-0 kyrs BP).

In PalMod at AWI (PalMod-1-3-TP1 and TP3) a suite of transient and time slice simulations has been conducted (Gong et al., 2018). Following a novel synthesis to assess the impact of combined ice sheet and CO_2 changes on the AMOC stability (Zhang et al. 2017) as part of a new working group within PMIP4 that is coordinated at AWI, experiments with MPI-ESM-LR and the AWI-ESM applied prescribed ice sheets for present day, 15.2 ka BP and LGM according to GLAC-1D (Tarasov et al., 2002, 2012) configurations. The simulations tested the impact of changes in ice sheet configuration, greenhouse gas concentrations, freshwater perturbations and orbital parameters on the stability characteristics of the AMOC within the glacial-interglacial phase space, with special emphasis on the potential for abrupt climate changes during the deglacial phase until the Bølling/Allerød interstadial warm phase. The investigations have shown that the deglacial AMOC in MPI-ESM largely exhibits mono-stable behavior and that the MPI-ESM is relatively insensitive to North Atlantic freshwater perturbations compared to the AWI-ESM.

By means of the modular ESM approach at AWI (ESM Tools, Cristini et al., in prep.) we will use the AWI-ESM as the working horse for future investigations within PalMod. This in particular includes the fully coupled AWI-ESM/PISM model, which is currently in the final phases of technical testing. At AWI this model will serve as the primary platform for the final leg of PalMod-Phase 1.

The GFZ (PalMod 1-1-5 and 1-2-4) utilized VILMA to reconstruct the glacial-isostatic adjustment (GIA) as the solid-Earth component in PalMod. Using model ensembles, the variability of relative sea level and paleo-topography during the last glacial cycle was analyzed under a number of aspects. Several model ensembles with different solid-earth and glacial-history parameterizations were generated. (1) For the analysis of the sea-level and paleo-topography variability in the Andaman Sea, a model ensemble with 125 statistically distributed members that differ in 1D viscosity structure (lithospheric thickness and viscosities of the upper and lower mantle) was computed. Results show a sea-level variability of around 1 m (std. dev.) and the opening of the Singapore Strait was reconstructed. (2) 3D viscosity-distributions – derived from seismic tomography models and geodynamic constraints – were applied to analyze the effect of 3D earth-structure in order to develop a reference 3D earth structure. (3) A statistical method to validate reconstructions of the late-glacial relative sea-level was applied to the ensemble runs (Latinovic et al. 2018). The left Figure 4 represents the ensemble mean of reconstructed relative sea-level at LGM and the right one is the fit of each ensemble member against set of sea-level indicators.

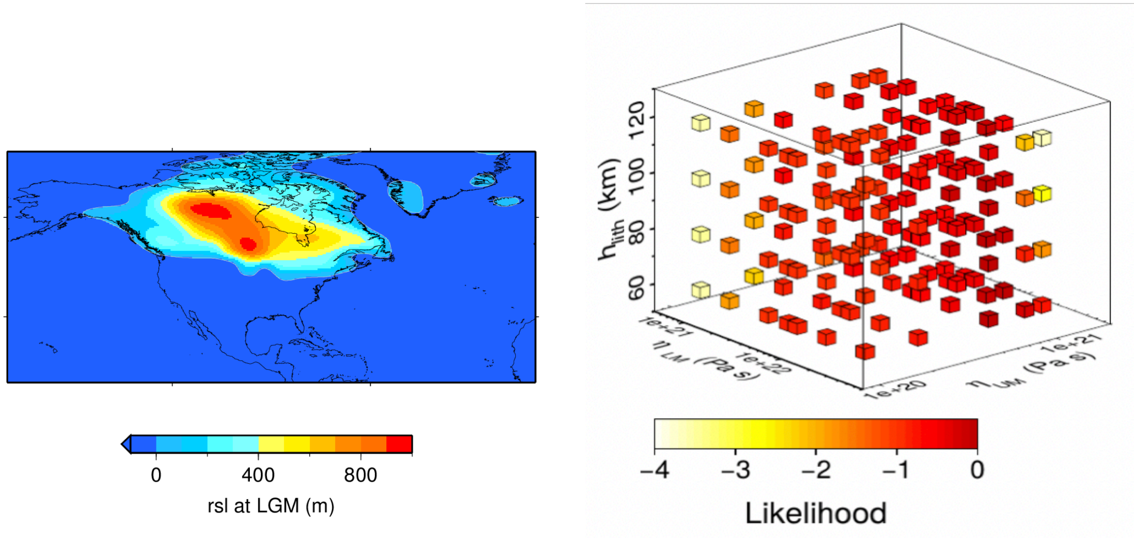

Fig. 4: Left: Ensemble mean of relative sea level (rsl) at the Last Glacial Maximum in the region of Hudson Bay. Right: 3D presentation of model ensemble with 140 members varying in lithosphere thickness (hlith) and upper- and lower-mantle viscosity (ηUM , ηLM). The color scale indicates the fit to the considered set of shallow-water shells of Hudson bay region.

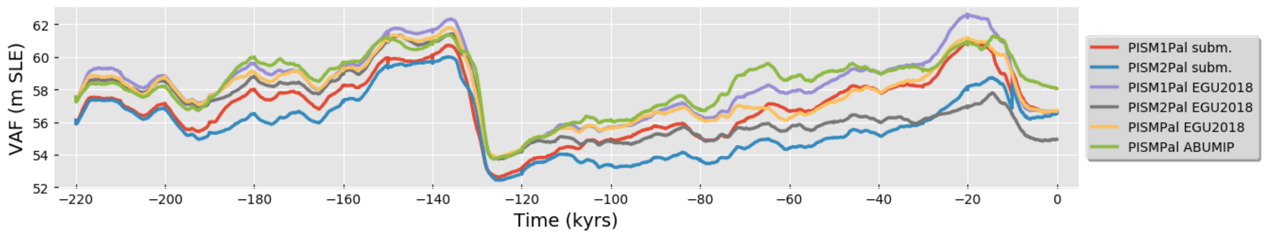

Fig. 5: Time series of the Antarctic Ice Sheet volume above floatation in meter sea-level equivalent (SLE) for the set-ups PISM1Pal and PISM2Pal as submitted to ISMIP6/InitMIP-Ant (subm.) and the identical set-ups rerun after major PISM bug fix (presented at EGU2018) as well as the new set-ups PISMPal as presented at EGU2018 and further improved for the ABUMIP submission.

In order to access grounding line dynamics in the PISM model in coarse resolution (16km) the AWI glaciology group (PalMod-1-2-TP1) has participated in two international model intercomparison projects (MIPs) that are based on the spin-up simulations submitted last year to ISMIP6/InitMIP-Ant (Nowickie et al., 2013) called ABUMIP and LARMIP. ABUMIP (Antarctic BUttressing Model Intercomparison Project) investigates the end-member of ice-shelf buttressing, the total loss of ice shelves. This enables gauging the sensitivity of different ice sheet models with respect to grounding-line retreat, as a function of basal sliding, isostasy, resolution, model physics and other model parameters. The ice sheet response to prescribed changes in shelf ice basal melting and thus grounding line dynamics is also investigated in LARMIP (Linear Antarctic Response to basal melting – Model Intercomparison Project). Due to serious problems effecting the reproducibility of the simulations in PISM versions stable v0.7.3 and stable v1.0 prior to March 2018, a recalibration of our set-ups for ISMIP6 became inevitable (still ongoing). A comparison of ice sheet volume time series for the ISMIP6 spin-up prior and after the bug fix is shown in

Fig. 5. We spent about three months in 2018 to investigate this particular bug. Unfortunately, the most recent versions of PISM (v0.7.3 and v1.0) still contain a number of issues effecting the reproducibility of model results and model restarts that need to be resolved. The work is further delayed by one month due to the parental leave of Dr. Thomas Kleiner (Jul. 2018).

ABUMIP: http://www.climate-cryosphere.org/wiki/index.php?title=ABUMIP-Antarctica

LARMIP: https://www.pik-potsdam.de/research/earth-system-analysis/models/larmip

References:

Cristini, L. et al.: Earth System Modelling Tools, manuscript in preparation for Geosc. Model. Dev.

Gong, X., Lembke-Jene, L., Lohmann, G., Knorr, G., Tiedmann, R., Zou, J.J., and Shi, X.F.: Enhanced North Pacific deep-ocean stratification by stronger Intermediate water formation during Heinrich Stadial 1, Nature Communications, in review, 2018.

Latinović, M., Klemann, V., Irrgang, C., Bagge, M., Specht, S., and Thomas, M.: A statistical method to validate reconstructions of late-glacial relative sea level – Application to shallow water shells rated as low-grade sea-level indicators, Clim. Past Discuss., doi:10.5194/cp-2018-50, in review, 2018.

Peltier W.R., Argus, D.F., and Drummund R.: Space geodesy constrains ice age terminal deglaciation: The global ICE-6G_C (VM5a) model, J. Geophys. Res. B, 120, 450-487, doi:10.1002/2014JB011176, 2015.

Tarasov, L. and Richard Peltier, W. (2002), Greenland glacial history and local geodynamic consequences. Geophysical Journal International, 150: 198-229. doi:10.1046/j.1365-246X.2002.01702.x.

Tarasov, L., S. Dyke, R. M. Neal, W. Peltier (2012), A data-calibrated distribution of deglacial chronologies for the North American ice complex from glaciological modeling, Earth and Planetary Science Letters, 315–316, 30-40. doi:10.1016/j.epsl.2011.09.010.

Zhang, X., Knorr, G., Lohmann, G., and Barker, S: Abrupt North Atlantic circulation changes in response to gradual CO2 forcing in a glacial climate state, Nat. Geosc., 10 (7), 518-523, doi:10.1038/ngeo2974, 2017.

Project: **1030**

Project title: **PalMod WG2**

Project lead: **Victor Brovkin**

Report period: **2017-01-01 to 2017-12-31**

WG2 of PalMod aims at understanding and quantifying feedbacks between biogeochemistry and climate during glacial cycles. Four work packages are focused on marine carbon cycle, terrestrial processes, CH_4 cycle, and the dust cycle. Scientific challenges include reproducing the glacial CO_2 cycle with comprehensive ESMs, understanding of rapid changes in atmospheric greenhouse gas concentrations during abrupt climate changes, and reconstructing atmospheric lifetime of CH_4 using a coupled atmospheric chemistry model.

PalMod WG2 contains work packages WP2.1 "Marine carbon cycle", WP2.2 "Terrestrial carbon cycle", WP2.3 "Methane cycle", and WP2.4 "Dust cycle".

Internal reallocation of computation time

Over the course of 2018 it became clear that computational resources requested for some parts of Palmod WG2 / bm1030 were not required after all, while other parts had higher demands than originally foreseen.

Overall, this led to a fairly good usage of the resources granted, though they were partly used for other purposes than originally envisaged:

WP 2.1 at CAU could not perform the planned experiments with Metos3D/HAMOCC, due to ongoing developments of Metos3D.

WP 2.2 at MPI-M could not perform the intended recalibration of the ECHAM6 atmosphere model, as the problems with soil thermal fluxes are still not sufficiently solved to invest the time into atmosphere model calibration

WP 2.1 at MPI-M had to perform additional experiments to investigate the effects of cloud parameters and freshwater hosing on the ocean circulation, as it became clear during 2018 that the modelled glacial circulation in MPIOM does not fit proxy data well and will likely prevent the storage of sufficient amounts of CO_2 in the deep ocean.

WP 2.1 "Marine carbon cycle", CAU Kiel

Unfortunately, a number of the planned experiments for 2018 at CAU could not be completed so far. First, none of the planned Metos3D/HAMOCC simulations with the 1° MITgcm transport matrix could be performed, due to ongoing developments of Metos3D in WG4. Second, the planned transient simulations of the deglaciation using MPI-ESM were not yet started, because the simulated LGM meridional overturning circulation in the Atlantic is currently too deep compared to reconstructions, due to a warm bias in the Southern Ocean which weakens the Antarctic bottom water formation. This ocean circulation bias would also lead to biased carbon cycle results; the WP2.1 group at MPI-M is currently working on a solution to achieve a more realistic LGM overturning circulation using freshwater hosing. Moreover, the postdoc at CAU was on parental leave from June 7th until September 6th, 2018.

On the upside, the planned MPIOM/HAMOCC sensitivity experiments with respect to particle ballasting in response to glacial–interglacial dust deposition changes have been completed and the results are currently under revision in GMD (Heinemann et al., 2018). It turned out, however, that the comparison of particle ballasting effects versus iron fertilization effects associated with the glacial–interglacial dust deposition changes are flawed in our MPIOM/HAMOCC model setup, because the dust deposition field used in HAMOCC (Mahowald et al. 2006) leads to high iron concentrations relative to nitrate concentrations in the Southern Ocean already under modern/interglacial conditions, so that non-diazotroph phytoplankton growth is nowhere iron limited but nitrate limited everywhere. Hence, additional iron input during glacial conditions does not lead to fertilization of phytoplankton growth. The exception are cyanobacteria (diazotrophs), which, unlike non-diazotroph phytoplankton, are not limited by the least available nutrient (Ilyina et al., 2013), but whose growth rate is proportional to the product of phosphate, light, and iron limiting functions (Paulsen et al., 2017). Hence, the additional iron input during glacial conditions does not lead to enhanced phytoplankton growth and organic matter export in the Southern Ocean, as suggested by the traditional iron hypothesis (Martin 1990), but only leads to enhanced cyanobacterial growth, organic matter export and consequently enhanced ocean CO_2 uptake in the tropics (Fig. 6).

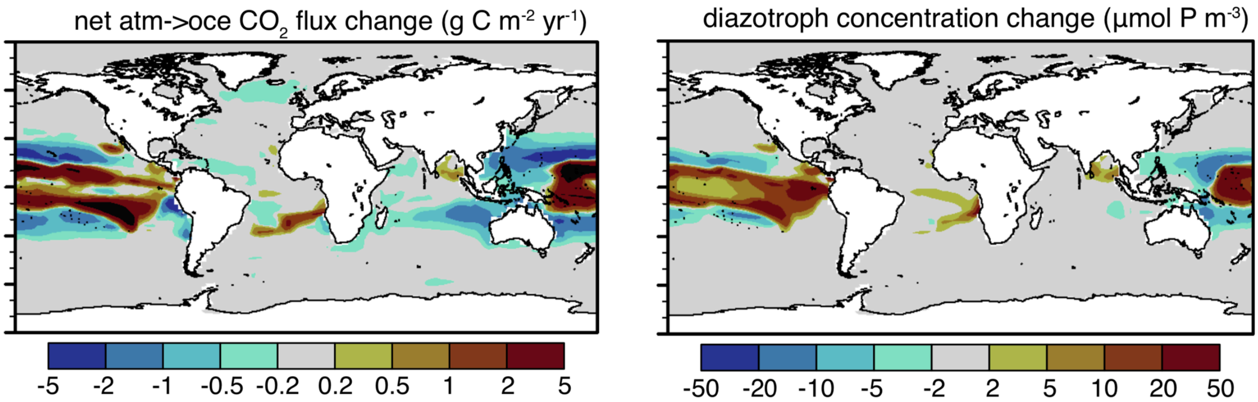

Fig. 6: Change of the net atmosphere–ocean CO2 flux (left; positive into the ocean) and of surface cyanobacteria (diazotroph) concentrations (right) in response to the addition of iron associated with the enhanced dust deposition during the LGM. Note the lack of ocean–atmosphere CO2 flux changes in the Southern Ocean.

Some of the remaining computation time on Mistral for 2018 will be used to redo the modern control simulations and LGM dust sensitivity experiments with a new dust deposition estimate for modern and LGM conditions (Albani et al., 2016); since the new estimate suggests that less dust is deposited in the Southern Ocean for modern conditions compared to the dust deposition field of Mahowald et al. (2006), it is anticipated that the Southern Ocean will be iron limited in the new simulations and that we will see an effect of iron fertilization and an anomalous ocean CO_2 uptake in the Southern Ocean in response to enhanced LGM dust deposition.

WP 2.1 "Marine carbon cycle", MPI-M

modelling oceanic stable carbon isotope 13C

A wealth of data exists on the past changes of the marine stable carbon isotopic signal $\delta^{13}C$, which is useful to constrain changes of the ocean circulation. To directly compare modelled oceanic $\delta^{13}C$ to data, we have implemented an advanced representation of 13C in MPI-ESM. To validate the new 13C module, we have carried out low-resolution (LR) stand-alone model (MPIOM/HAMOCC) simulations. Specifically, we first conducted the pre-industrial control simulation, with atmospheric $\delta^{13}CO_2$=-6.5‰. Next, we account for Suess effect (that is, the gradual decrease of $\delta^{13}CO_2$ due to isotopically light fossil fuel CO_2 input) and continued the run till year 2010. Our modelled $\delta^{13}C$ of particulate organic carbon (POC) and that of inorganic carbon (DIC) captures the major features of the observational data, as is shown in Figure 7 and 8. One visible disagreement between model and data is that in the interior of the equatorial Pacific Ocean (Figure 8), the modelled $\delta^{13}C_{DIC}$ is much lower compared to data. This is caused by the nutrient trapping problem in MPI-ESM, which is mainly related to the unresolved dispersion and/or circulation processes in this region. Since the biological fractionation during photosynthesis is still under debate (Keller and Morel, 1999), we are running simulations with another parameterisation of biological fractionation by Laws et al. (1995). The parameterisation of biological fractionation used in Figure 7 and 8 are from Popp et al. (1989).

sensitivity study concerning cloud parameters

We applied the 13C model to the LGM period. The modelled LGM $\delta^{13}C$ does not capture the strong vertical gradient shown in the $\delta^{13}C$ proxy data, see Figure 9a and 9b. This is mainly due to the deep boundary (3500 meters north of 30°N in the Atlantic Ocean) between the two upper NADW cell and the lower AABW cell of AMOC in the model. The reason for the deep boundary between the two cells of AMOC is that in the coarse-resolution (CR) mode of the current MPI-ESM, the surface ocean temperature in the Southern Ocean has a warm anomaly of 4-5°C in the pre-industrial control run. Consequently, the ice volume in the Southern Ocean is small and the AABW formation is thereby too little. To decrease the warm SST anomaly in the Southern Ocean, we have conducted sensitivity studies concerning several cloud parameters that could theoretically cool down the climate in the high latitude regions. However, model results show that the Southern Ocean SST and the state of is only marginally affected. Correspondingly, the $\delta^{13}C$ distribution hardly differ among these sensitivity experiments.

LGM freshwater hosing experiments

To obtain different LGM ocean overturning circulation states, we conducted freshwater hosing experiments. Specifically, we hose in the North Atlantic between 45° and 65° N with a surface freshwater flux of 0.1, 0.2, 0.25, 0.3, 0.35, 0.4 Sv, respectively. The strength of the LGM NADW cell decreases from 26 Sv (no hosing) to 7 Sv (with freshwater hosing flux of 0.4 Sv). Correspondingly, $\delta^{13}C$ in the interior of the Atlantic significantly decreases (Figure 9c). However, in each of these experiments the modelled $\delta^{13}C$ in the south sector of the Atlantic is higher compared to data. The main reasons are two-fold. First, the AABW cell remains weak in these runs due to warm bias in the Southern Ocean. Second, the primary production in the LGM Southern Ocean is lower than the pre-industrial state, whereas LGM nitrogen isotope proxy data suggest the opposite.

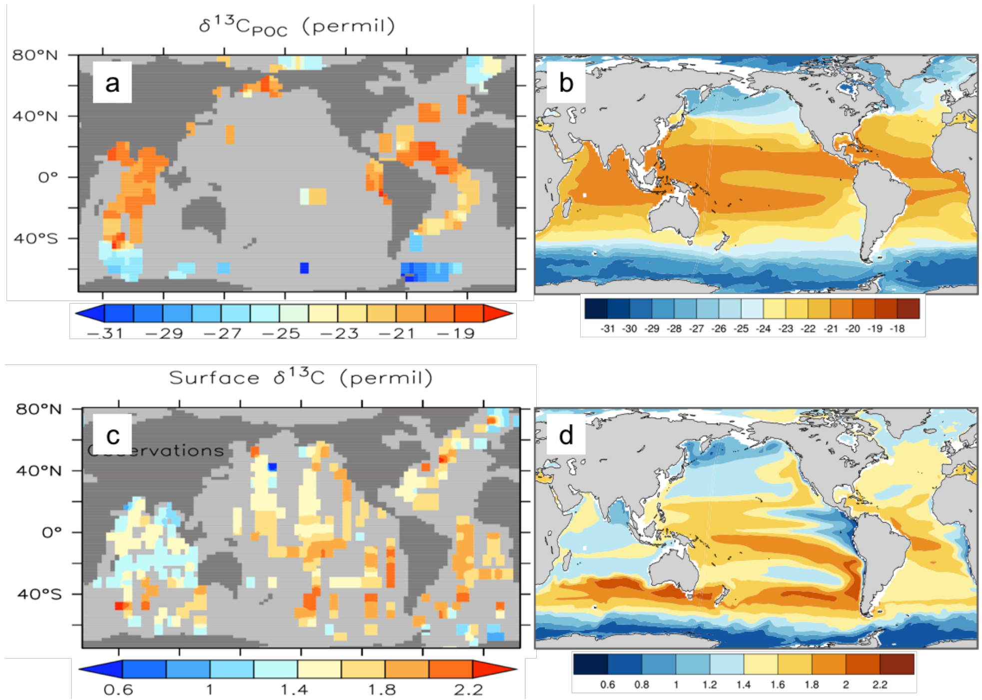

Fig. 7: Comparison of surface (that is, the depth-average of the top 100 meters) δ13CPOC (upper row, in ‰) and δ13CDIC (lower row, in ‰) distributions of 1990s between observations (left column) and model results (right column). The figures of observations are from Schmittner et al. (2013).

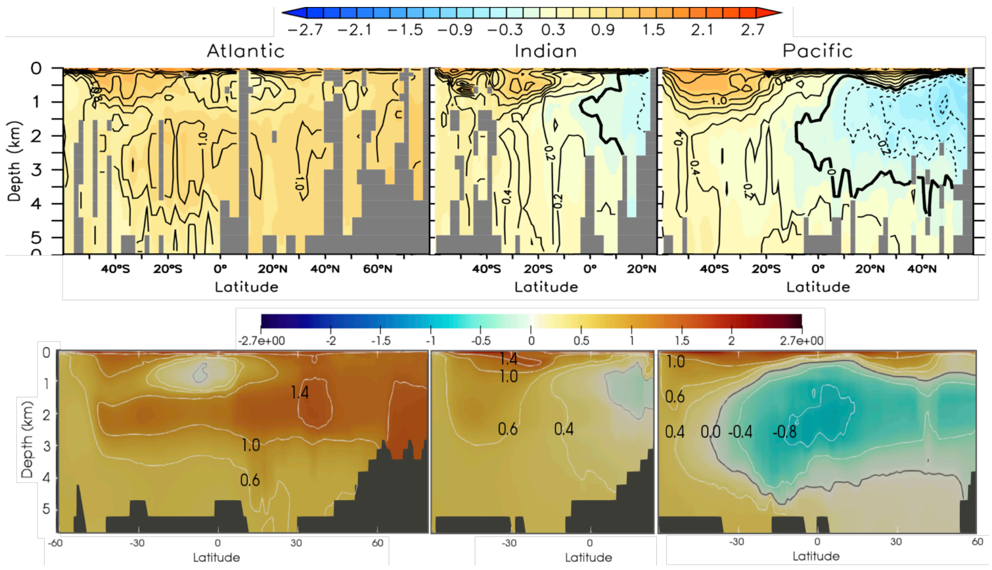

Fig. 8: Comparison of zonally-averaged δ13CDIC (in ‰) distributions of 1990s between observations (upper row) and model results (lower row) in the Atlantic, Indian and Pacific oceans. The figures of observations are from Schmittner et al. (2013).

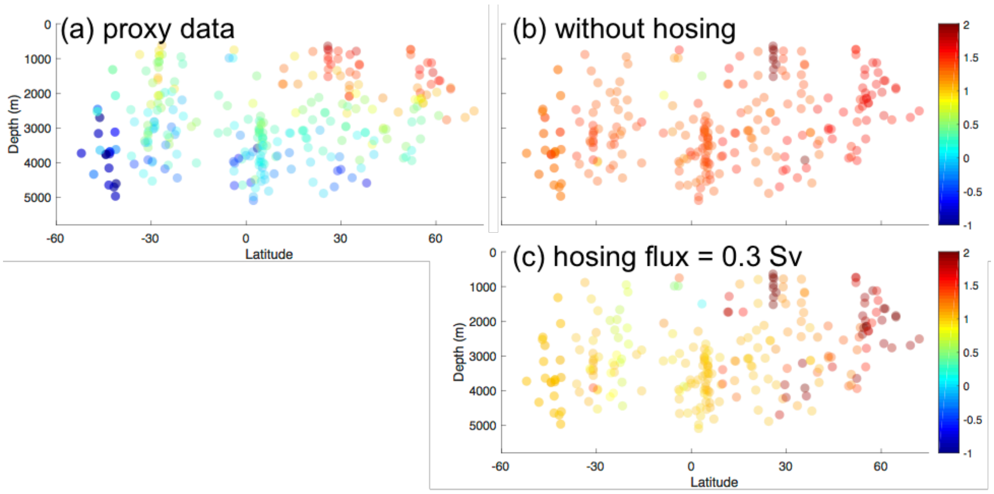

Figure 9: Comparison of LGM δ13CDIC (in ‰) between proxy data (left) to model results (right) that are sampled at the sediment core location in the Atlantic Ocean.

WP2.2 "Terrestrial Carbon Cycle", MPI-M

WP2.2 mainly planned to use computation time at DKRZ to re-calibrate the atmospheric model ECHAM6 to lessen the biases with regard to atmospheric temperature, if the JSBACH permafrost module was switched on. However, we were so far unable to address the severe problems in thermal fluxes within the submodel, leading to wrong thaw depths, which we reported last year.

Unfortunately, we were so far not able to address these issues and therefore postponed the re-calibration of the atmospheric model to 2019.

We did, however, perform a transient experiment from LGM to PI to assess the land carbon cycle under transient conditions including a changing land-sea mask.

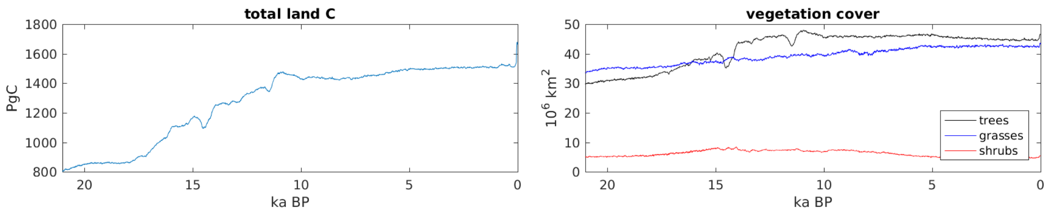

Fig. 10: Total land carbon (left) and vegetation cover (right) from LGM to PI. Total land C nearly doubles from LGM to PI, while grass cover increases roughly linearly and tree cover shows the strongest changes during the deglaciation proper.

Here, the total land C stock roughly doubles between LGM and the present, with the bulk of the change occurring during the deglaciation (Fig. 10, left). Vegetation cover changes (Fig. 10, right) showed small changes in shrub coverage, a slow expansion in the area covered by grasses, and a stronger increase in the area covered by trees. The latter change mainly occurs between 17 ka BP and 10 ka BP, with tree cover slowly decreasing afterwards.

Further model development and experiments in 2018 addressed the effects of fire on the vegetation distribution. As the distribution of lightning changes with the drastic climatic changes between LGM and PI, we used the lightning model required in WP 2.3 to test the effects of interactively simulated lightning as opposed to prescribed lightning as a fire ignition source and adapted the dynamic vegetation model to the resulting changes in fire distribution.

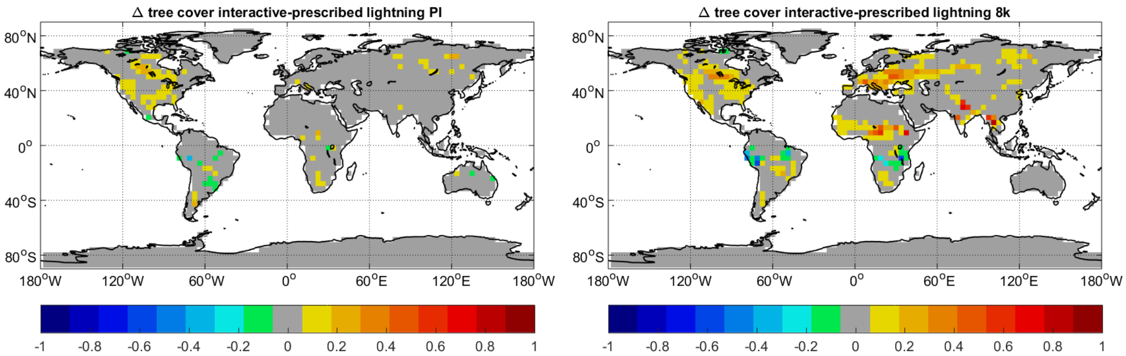

Fig. 11: Difference in tree cover between prescribed modern and interactively simulated lightning distribution for preindustrial (left) and 8 ka BP (right)

Overall, the changed fire parameterisation leads to a slight increase in tree cover for the preindustrial state (Fig. 11, left), but changes are substantially larger for the early Holocene (Fig. 11, right). A transient experiment to assess the effect on overall C cycling from LGM to present is scheduled for the last quarter of 2018.

WP 2.3 "Methane cycle" (MPI-M)

In 2018 we developed 3 new model components for methane cycling in MPI-ESM. We developed a model to diagnose methane emissions from Termites, we extended the SPITFIRE fire model within JSBACH to diagnose wildfire-related methane emissions, and we integrated the atmospheric sink of methane in MPI-ESM, developed by MPI-C in their part of the project as detailed in the next section.

Model development required numerous short experiments. We also performed time slice experiments for selected time slices from LGM to the present to determine methane emissions and atmospheric concentrations as a preparation for an initial transient experiment for the entire time from LGM to PI, to be performed in the last quarter of 2018.

The modelled methane emissions compare well to global assessments for the present day, and the time slice experiments generally show the expected pattern: Roughly a doubling of methane emissions between LGM and Holocene, higher methane emissions in the early Holocene and at present than at mid-Holocene. Also, wetlands are the dominant source of methane (Figure 13). A publication on the time slice experiments is near ready for publication.

Atmospheric methane concentrations –determined using the atmospheric sink module newly developed in cooperation with MPI-C -- (Fig. 18) show the expected pattern, mainly reflecting the source distribution. However detailed analysis shows some biases in both emissions and atmospheric sink, needing to be addressed in 2019.

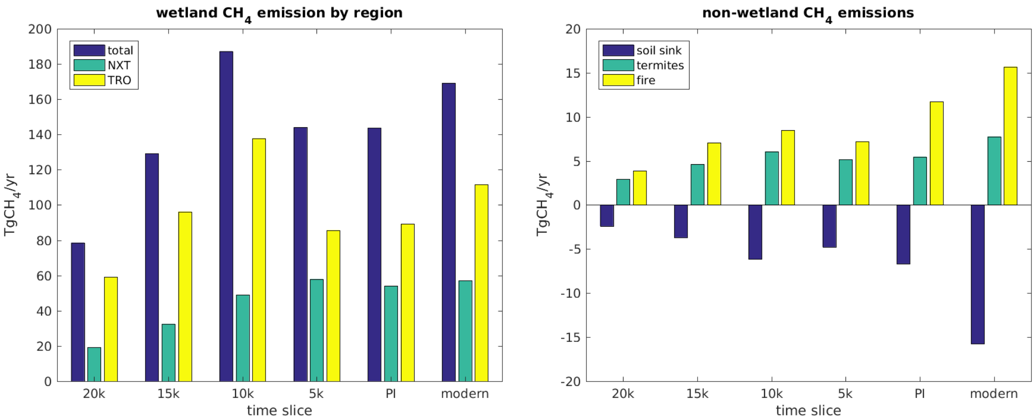

Fig. 12: Terrestrial methane emissions from wetland (left) and non-wetland (right) methane sources from the CH4 emission model. Present-day emissions compare well to methane assessments.

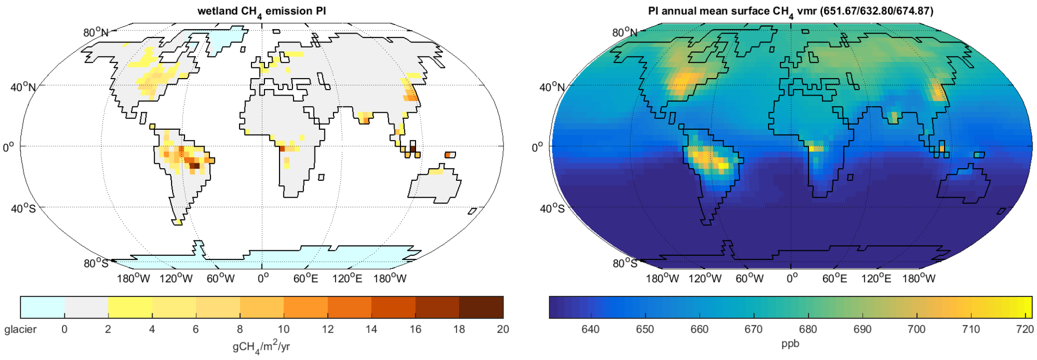

Fig. 13: Wetland methane emissions (left) and near surface atmospheric concentration (right) for preindustrial climate conditions.

In comparison to ice cores (Fig. 14), modelled atmospheric concentrations for 20k, 10k, and PI show a general model bias towards high latitude emissions and a general overestimate of emissions for the Holocene – these biases will be addressed in 2019.

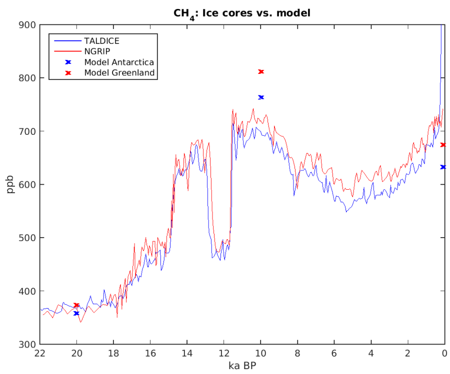

Fig. 14: Ice core methane concentrations from Antarctica and Greenland (blue and red lines, respectively) and modelled concentrations at the sites for 20k, 10k, and PI.

WP 2.3 "Methane cycle" (MPI-C)

Atmospheric oxidative capacity and methane lifetime

Within the project year 2018, we have continued numerical experiments on past atmosphere oxidative capacity (and therefore methane lifetime), with a deeper focus on the secondary factors controlling its variations. Such is necessary in order to ascertain that variations in the tropospheric lightning NO_X emissions, as we establish in our sensitivity simulations, are indeed the only principal factor controlling CH_4 lifetime in the past natural atmospheres. Using the "dynamic" setups of the EMAC AC-GCM for the Last Glacial Maximum (LGM) we have quantified the uncertainties in the radicals budgets related to atmospheric domain exchange, i.e. caused by variations in transport and mixing terms, and their interconnection with the kinetic chemistry. We find, for instance, that allowing free (i.e. not relaxed towards MPI-ESM-P lgm_r1i1p1-P experiment (Giorgietta et al., 2013), as in "regular" setups) stratospheric dynamics of EMAC results in marginal change in tropospheric O_3 (−0.3%), OH (+0.9%) and NO_X (+1.9%) burdens, with no substantial effect on stratosphere-troposphere transport of ozone (STT). Similarly, doubling of deposition velocity over land results in minor increase in dry deposition of O_3 (2.7‰) only in tropospheres with very low abundances of NO_X. In contrast, oxidants' burdens vary substantially in response to changes in reactive C and N emissions from the surface and lightning sources. Figure 15 shows an overview of the sensitivity experiments we have conducted for LGM together with reference simulations for the present-day (PD) conditions.

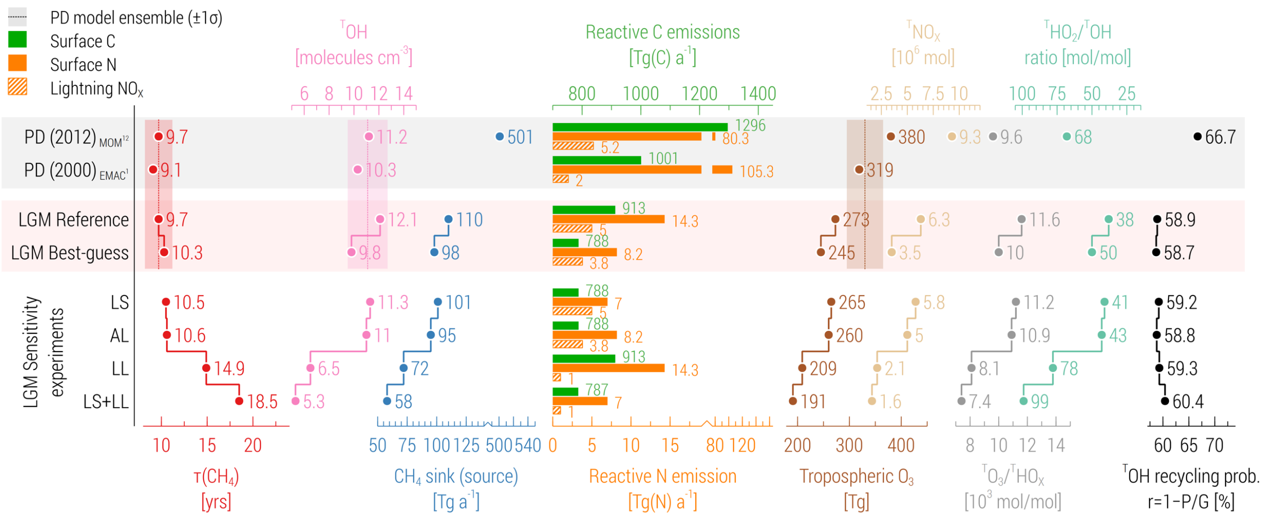

Fig. 15: Overview of the model experiments with EMAC LGM on sensitivity of atmospheric CH4 lifetime to the reactive C and N emissions. Symbols denote the tropospheric averages of respective simulated characteristics (horizontal scales). Shaded rows highlight LGM Reference and „best-guess" setups (red) and results for some PD simulations (grey) with EMAC for comparison. Horizontal bars show the reactive N and C emission fluxes probed in different setups. Vertical dotted lines and shaded areas denote the multi-model estimates for selected characteristics for PD. Note that for the reference and „best-guess" setups the model predicts similar τCH4 and a low equivalent CH4 emission flux of 95–110 Tg(CH_4)/yr.

In order to explicate covariations of lightning NO_X emissions with tropospheric OH, NO_X and O_3 abundances, we performed simulations with extensive budgeting of these compounds. As result, we identified an important linking O_3 STT and equilibration of tropospheric O_3 burden: lack of NO_X-driven recycling of ozone (e.g. due to low free-tropospheric NO_X) is compensated through increased net STT (see Fig. 16). Whilst PD conditions render troposphere as net chemical producer of O_3, natural colder tropospheres (here LGM) should act as net sink; the importance of stratospheric O_3 and increasing STT in this case for tropospheric oxidative capacity is cardinal. Importantly, the sensitivity of O_3 abundance (and hence "primary" production of OH, the principal CH_4 removal agent) to the available NO_X in the troposphere is substantially higher than in previous studies (e.g. Murray et al., 2014; Valdez et al., 2005). We conclude that the cause for this is much more simplified chemical mechanisms used in these studies, in contrast to that in EMAC.

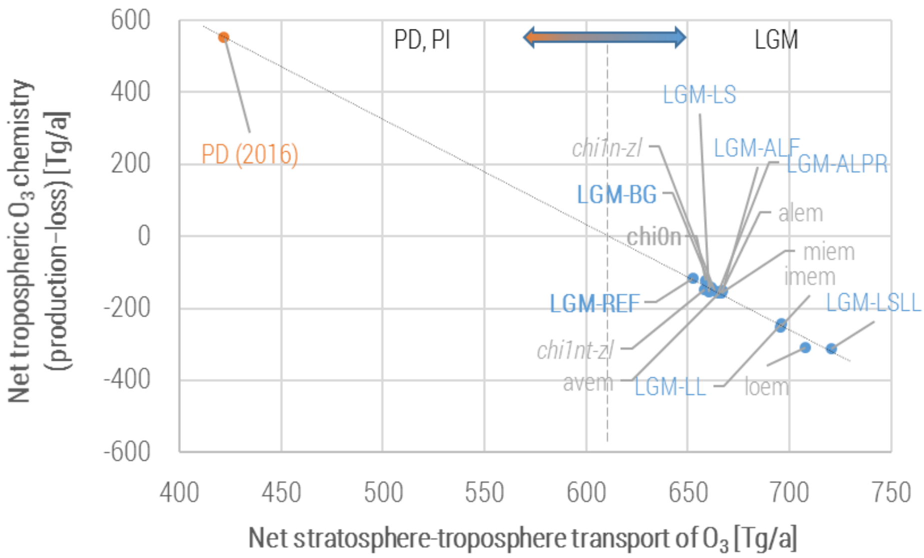

Fig. 16: Correspondence between net photochemical O3 turnover and net STT simulated in EMAC for PD (red symbols) and LGM conditions (blue symbols, grey captions denote sensitivity simulations with extended budgeting of atmospheric oxidants). Near-linear relationship denotes similar sensitivity of tropospheric O3 to NOX abundances. Dashed vertical line denotes the STT term at which photochemical production and sink of O3 are in equilibrium. Notably, in natural LGM atmosphere, tropospheric domain acts as net chemical sink of O3, in contrast to the PD conditions.

WP2.4 "Dust cycle" is focused on the interactive simulations of dust sources and depositions during the last deglaciation. The interactive model of dust emission, transport, and deposition as well as a modulator of the radiative forcing will be an intrinsic part of ESM and EMICs simulations in WG1. In addition, the biogeochemical role of dust as a forcing for marine biogeochemistry through Aeolian transport and deposition of micro-nutrients (iron) will be explored together with WP2.1. WP2.4 assigned work in this request is performed at TROPOS.

Project objectives

The overall objective of the planned simulations is to optimize the dust production module with regard to its applicability for climate simulations and to review the representation of predominant dust source types. The individual tasks are: (1) Assessment and optimization of the dust production model in ECHAM6-HAM2 (global scale; simulations performed at DKRZ). (2) Sensitivity study (continuing) regarding spatial and temporal resolutions (model grid spacing), and configurations of the dust production module.

Work achieved until 2018-10-31

In order to ultimately aim for a computationally efficient dust module implemented in the MPI-ESM (core similar to ECHAM6-HAM2 which is used here), the following tasks were carried out:

Assessment and optimization of the dust production model in ECHAM6-HAM2 (global scale, simulations performed at DKRZ). In favour to reduce the computational costs due to the interactively called dust modules, the following approach was suggested and elaborated during the reporting period: 10 years per century will be simulated with interactive dust, which then will be compiled into a climatology to be called throughout the remaining 90 years per century. To achieve this, the following steps have been carried out:

Set up of "dust only" ECHAM-HAM version with JSBACH-based dust source description. This model configuration uses a reduced aerosol model for which only two of the seven available modes are populated, i.e. the insoluble accumulation and coarse mode. The dust sources are computed online as described by Stanelle et al. (2014), instead of being read-in from an external data set. This allows for adaptation to land cover changes. Test simulations have revealed that the model is not in radiative equilibrium (Fig. 17, Tab. 1) and thus requires tuning in order to obtain radiative balance at the top of the atmosphere. However, this task is not feasible in the framework of PalMod WP2.4 on its own.

Set up of "dust only" ECHAM-HAM version with JSBACH-based dust source description. This model configuration uses a reduced aerosol model for which only two of the seven available modes are populated, i.e. the insoluble accumulation and coarse mode. The dust sources are computed online as described by Stanelle et al. (2014), instead of being read-in from an external data set. This allows for adaptation to land cover changes. Test simulations have revealed that the model is not in radiative equilibrium (Tab. 1, Fig. 17) and thus requires tuning in order to obtain radiative balance at the top of the atmosphere. However, this task is not feasible in the framework of PalMod WP2.4 on its own.

Model configuration	ECHAM6 with full HAM T63L47	ECHAM6 with full HAM T63L31	ECHAM6 with dust-only HAM T63L31	ECHAM6 with dust-only HAM T31L31
F_{net} @ TOA	0.57	0.62	1.77	1.92

Table 1: Top of atmosphere radiative (im)balance of ECHAM6-HAM2 in different configurations and spatial resolutions. Test were conducted with present-day climatological SSTs and ran for 5 years each.

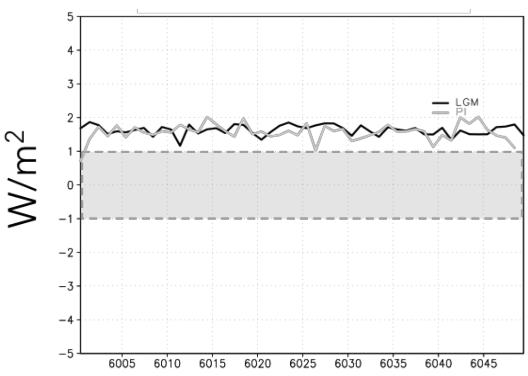

Fig. 17: Radiative balance (incoming SW + outgoing LW) at TOA for two simulations with T31L31 ECHAM-HAM

'dust only': Pre-industrial conditions (grey) and Last Glacial Maximum (LGM) conditions (black). The radiative imbalance is higher than the acceptable range of +/- 1 W/m2 (grey shading).

Implementation of dust as a passive tracer without HAM in MPI-ESM. To achieve this, the following option is discussed predominantly: Implementation of a simplified dust emission module into MPI-ESM and a life-time based description for dust deposition. Sources are computed interactively based on JSBACH land cover accounting for changes in surface conditions relevant for Aeolian erosion as described above. In particular, all emitted dust is assigned to the coarse mode, which is the only dust tracer to be transported. For simplicity, the explicit calculation of wet and dry deposition as well as of sedimentation due to gravity are omitted in favour of a life-time based approach. To estimate dust life-time further sensitivity studies are planned.

Sensitivity study. In order to support (1) and ultimately verify the model's performance, sensitivity studies are carried out.

References:

Albani, S., Mahowald, N. M., Murphy, L. N., Raiswell, R., Moore, J. K., Anderson, R. F., McGee, D., Bradtmiller, L. I., Delmonte, B., Hesse, P. P., and Mayewski, P. A.: Paleodust variability since the Last Glacial Maximum and implications for iron inputs to the ocean, Geophysical Research Letters, 43, 3944–3954, 2016.

*Giorgetta, M. A., et al.: Climate and carbon cycle changes from 1850 to 2100 in MPI-ESM simulations for the Coupled Model Intercomparison Project phase 5, J. Adv. Model Earth Syst., **5**, 572−597, doi: 10.1002/jame.20038, 2013.*

Heinemann, M., Segschneider, J. and Schneider, B.: CO_2 drawdown due to particle ballasting and iron addition by glacial aeolian dust: an estimate based on the ocean carbon cycle model MPIOM/HAMOCC version 1.6.2p3, Geoscientific Model Development Discussions, DOI 10.5194/gmd-2018-137, 2018.

Ilyina, T., Six, K. D., Segschneider, J., Maier-Reimer, E., Li, H., and Núñez-Riboni, I.: Global ocean biogeochemistry model HAMOCC: Model architecture and performance as component of the MPI-Earth system model in different CMIP5 experimental realizations, Journal of Advances in Modeling Earth Systems, 5, 287–315, 2013.

Martin, J. H.: Glacial-interglacial CO_2 change: The Iron Hypothesis, Paleoceanography, 5, 1–13, 1990.

Mahowald, N. M., Muhs, D. R., Levis, S., Rasch, P. J., Yoshioka, M., Zender, C. S., and Luo, C.: Change in atmospheric mineral aerosols in response to climate: Last glacial period, preindustrial, modern, and doubled carbon dioxide climates, Journal of Geophysical Research: Solid Earth, 111, 2006.

*Murray, L. T., et al.: Factors controlling variability in the oxidative capacity of the troposphere since the Last Glacial Maximum, Atmos. Chem. Phys., **14**, 3589−3622, doi: 10.5194/acp-14-3589-2014, 2014.*

Paulsen, H., Ilyina, T., Six, K. D., and Stemmler, I.: Incorporating a prognostic representation of marine nitrogen fixers into the global ocean biogeochemical model HAMOCC, Journal of Advances in Modeling Earth Systems, 2017.

Stanelle, T., Bey, I., Raddatz, T., Reick, C., and I. Tegen, Anthropogenically induced changes in twentieth century mineral dust burden and the associated impact on radiative forcing, J. Geophys. Res. Atmos., 119, 13.526-13.546, doi:10.1002/2014JD022062 , 2014.

*Valdes, P. J., Beerling, D. J., and Johnson, C. E.: The ice age methane budget, Geophys. Res. Lett., **32**, L02704, doi: 10.1029/2004GL021004, 2005.*

Project: **bu1029**

Project title: **PalMod WG3**

Project leader: **Andreas Hense/Florian Kapp (Uni Bonn), Gerd Schaedler/Marcus Breil (KIT), Bijan Fallah (FUB), Martin Werner/Alexandre Cauquoin (AWI)**

Reporting period: **1.1.2018 - 31.12.2018**

WP3.1-TP04 (Uni Bonn)

Already In 2017, an ensemble simulation for the Mid Holocene (MH, 6000 years before present) was performed on HLRE-3 using the state-of-the-art atmospheric climate model ECHAM6. The model was driven by ocean sea surface temperature and sea ice concentration fields from a previously performed transient simulation. The simulated wind fields were used in 2018 to set up a linear advection-diffusion model. Furthermore, the model results were utilized to estimate spatial covariance structures for the 2 meter temperature. These correlations are needed in order to correctly assess the mismatch between proxy data and the simulations. Figure 18 shows an example of the spatial correlations between the grid cells to a cell lying the atlantic stormtrack. The advective zonal transport of information is evident.

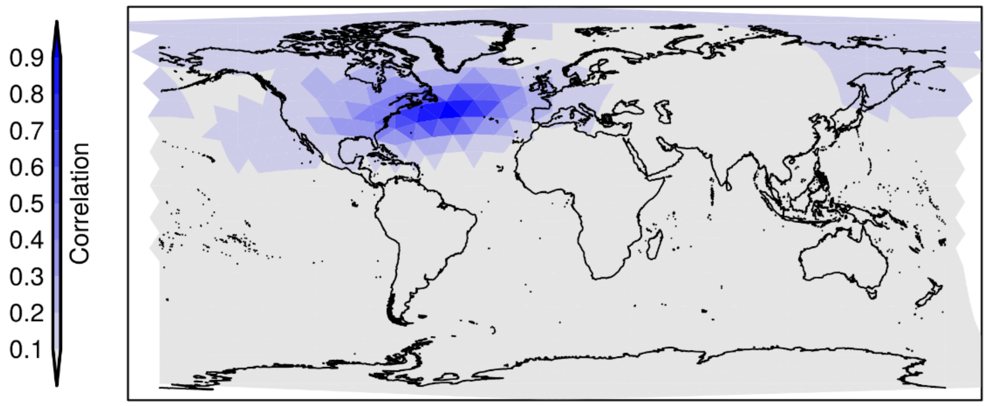

Fig. 18: Correlation structure of near surface temperature anomalies (here for a grid point in the North Atlantic) estimated from the internal variability of ECHAM6 simulations interpolated to the ICON triangular grid

In the remainder of 2018 the Eemian Interglacial (125,000 years before present) will be simulated using the coupled ocean-atmosphere climate model MPI-ESM (version 1.2.00p4). The Eemian was studied with complex climate models before.However, the last simulations were performed more than seven years ago with climate models of less complexity and coarser resolution (e.g. Fischer and Jungclaus, 2010; Robinson et al., 2011). Also, the final transient model runs within PalMod are expected to be simulated with MPI-ESM and will be initialized in the Eemian Interglacial. Thus, this simulation and proxy-data comparison willcontribute to this final goal. The model consists of the atmospheric component ECHAM6 (version 6.3.02p4),coupled to the land-vegetation model JSBACH, and the ocean model MPI-OM (version 1.6.2p3) including a biogeochemistry module HAMOCC. All submodels are linked via the OASIS3 coupler. ECHAM6 runs on a T63L47 grid, MPI-OM on GR15L40. The model is initialized with present day fields and spun up until the ocean reaches a steady state. The following hundreds of years are used in the analysis. The orbital parameters are set according to Berger and Loutre (1990). The land sea mask is unchanged as differences to present day sea levels are small (Cuffey and Marshall, 2000). The vegetation is initialized as the distribution of the recent climate and dynamically computed from JSBACH. As an innovation, the carbon cycle will be included such that the CO2 concentration is interactively calculated from the model.

References

Berger, André, and Marie-France Loutre. "Insolation values for the climate of the last 10 million years." Quaternary Science Reviews 10.4 (1991): 297-317.

Cuffey, Kurt M., and Shawn J. Marshall. "Substantial contribution to sea-level rise during the last interglacial from the Greenland ice sheet." Nature 404.6778(2000): 591.

Fischer, N., and J. H. Jungclaus. "Effects of orbital forcing on atmosphere and ocean heat transports in Holocene and Eemian climate simulations with acomprehensive Earth system model." Climate of the Past 6 (2010): 155-168.

Robinson, Alexander, Reinhard Calov, and Andrey Ganopolski. "Greenland ice sheet model parameters constrained using simulations of the Eemian Interglacial." Climate of the Past 7.2 (2011): 381-396.

WP 3.3 TP01 (AWI)

Used resources in 2018

We have produced 3 equilibrium simulations of 2000 years each (instead of the planned 1000 years). This represents almost 100,000 node hours. So, we have used the 60,000 node hours requested for the project bb1029 in 2018 and 40 000 additional node hours in other projects in which we are involved (ba0989, ab0246). As we work in very close collaboration with the PalMod WG1 group, and due to the lack of space in the WG3 working directory, we had the possibility to store the data in WG1 disk space.

Short summary of achieved results

We have performed 3 equilibrium simulations under pre-industrial (PI), Mid-Holocene (6k) and Last Glacial Maximum (LGM) conditions with the isotope-enabled version of MPI-ESM, called hereafter MPI-ESM-wiso. The water cycle is a key component of the Earth's climate system. One way to document its past evolution in order to test the models for future climate projections is to use the water stable isotopes $H_2{}^{16}O$, $H_2{}^{18}O$ and HDO. They are integrated of climate processes occurring in various branches of the hydrological cycle and are extremely useful to describe its past changes. Measured in the polar ice cores, the water stables isotopes (expressed hereafter in the δ notation as $\delta^{18}O$ and δD, with respect the Vienna Standard Mean Ocean Water standard V-SMOW) are used for past temperature reconstructions over the past glacial-interglacial cycles. In continental speleothems, they can be related to the past amount of precipitation. In marine sediments, the water isotope concentrations give access to the water mass changes. The simulation of the water isotope bodies in a coupled GCM is extremely powerful as it allows a direct model-data comparison for different climate periods. This is important for testing the hydrological cycle in the models and for better explaining fundamental links between the water cycle and the climate variability.

Figure 19 shows the global distribution of annual mean $\delta^{18}O$ values in precipitation under pre-industrial conditions as simulated by MPI-ESM-wiso. The comparison with the isotopic data (observations from GNIP stations (IAEA), ice core records and speleothems records) shows a very good agreement with a model-data slope of 0.85 (1 being the perfect fit) and a root mean squared error (RMSE) of 2.5‰. The modelled δ^{18}O-temperature gradient (0.63 ‰/°C; r^2=0.97) is also very close of the observed one (0.66 ‰/°C; r^2=0.95). This represents a slight improvement compared to the ECHAM5/MPIOM model enabled with water isotopes.

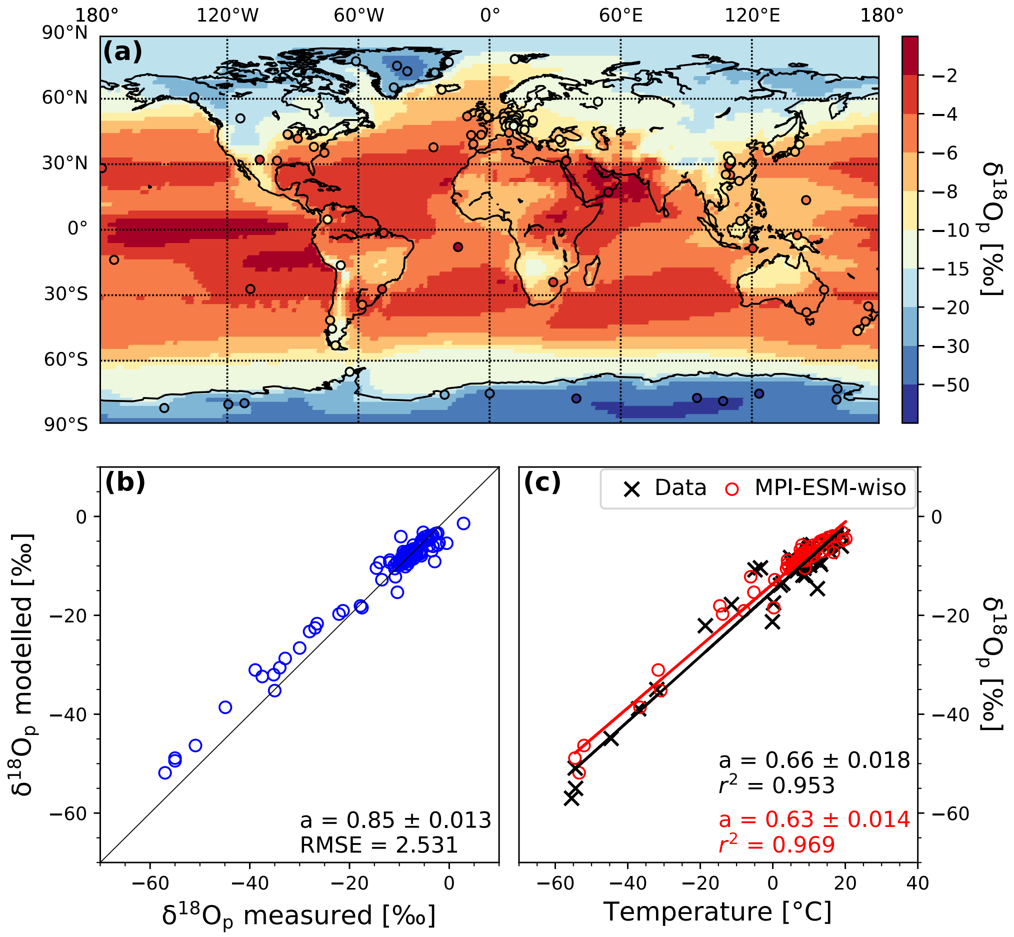

Fig. 19: (a) Global distribution of simulated (background pattern) and observed (colored dots) annual mean δ18O values in precipitation under PI conditions. (b) Modelled vs. observed annual mean δ18O at the different GNIP, speleothem, and ice core sites. (c) Observed (black crosses) and modelled (red circles) spatial δ18O-T relationship for the sites where the observed annual mean temperatures are below +20°C. The linear fits for the observed and modelled values are drawn as black and red lines respectively. For both (b) and (c), the slopes of the linear regression fits are given in the legends.

By simulating different time periods with an isotope-enabled model, it is possible to study the changes in δ^{18}O between two climatic periods and its relationship with climatic parameter as temperature, precipitation or salinity. For example, studying these changes between mid-Holocene and pre-industrial climate allows to examine the forced response to orbital and greenhouse gas forcing. The Figure 19 shows the modelled changes in δ^{18}O in precipitation between 6k and PI and a comparison with some observations from ice cores and speleothem records. At the high latitudes, the water isotope variations are mainly influenced by the changes in temperature while the 6k-PI δ^{18}O anomalies at lower latitudes are mainly driven by the changes in the amount of precipitation, especially over the Pacific Ocean on the Asian coast and over the East Indian Ocean. The model results agree relatively well with the available data. The largest deviations are found for speleothem data in the

Western USA and near the Rio Grande. This is not surprising because the isotopic composition of drip water archived in speleothems can be biased in several ways: variable and different from PI climate at a speleothem site, seasonal bias due to re-evaporation of precipitated water, additional fractionation between the drip water and the formation of calcite.

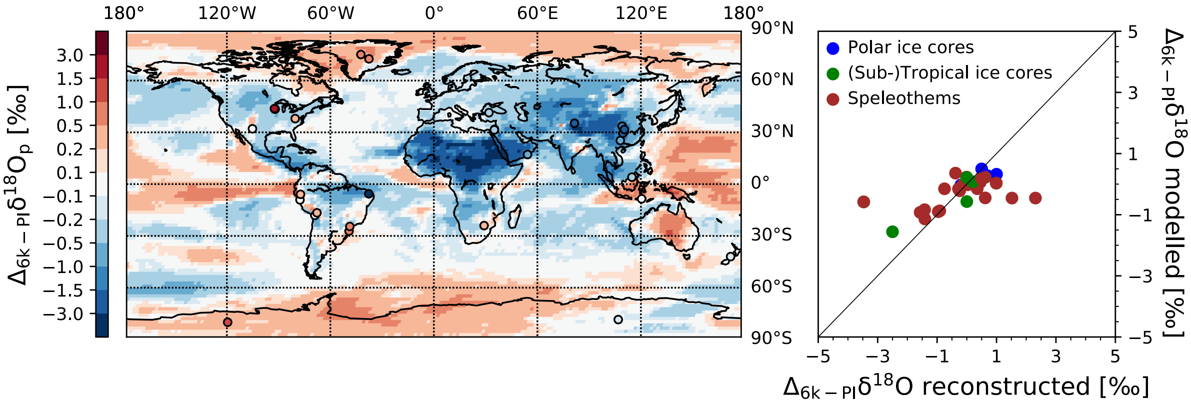

Fig. 20: (left) Simulated global pattern of annual mean $\delta^{18}O$ changes in precipitation between the Mid-Holocene and PI climate and comparison with reconstructed $\delta^{18}O$ changes in ice cores and in calcite speleothems (colored symbols). (right) Reconstructed $\delta^{18}O$ changes from ice cores and speleothems vs. simulated 6k-PI $\delta^{18}O$ anomalies at the same location.

A manuscript presenting these results is under preparation and will be submitted by the end of the year in Climate of the Past.

Concerning the LGM run, we have noticed that MPI-ESM seems to overestimate the land surface temperature, that means that the cooling between PI and LGM is not strong enough compared to the results from PMIP3 models. As there is a strong link between temperature and the isotopic composition of precipitation, the model overestimates the $\delta^{18}O$ in precipitation too (Fig. 20). Some discussion will be done about this issue in our AWI group.

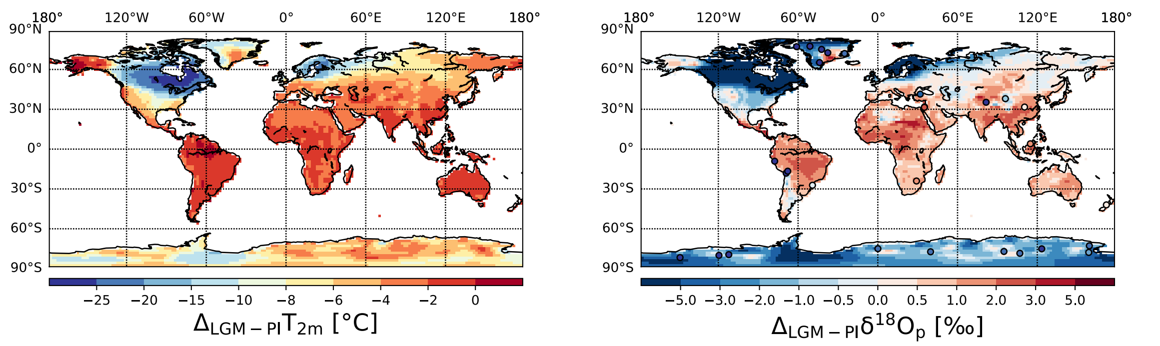

Fig. 21: Simulated LGM-PI annual mean changes in land surface temperature (left) and ⍰18O in precipitation (right).

WP 3.3 TP03 (KIT)

Stable isotopes of water are fractionated during phase transition, leading to different isotopic compositions in liquid, evaporated, condensed and frozen water. The distribution of stable isotope ratios in atmospheric water vapor and precipitation can therefore be used to draw conclusions about atmospheric conditions and the underlying physical processes. Since isotope ratios in precipitation from the past were recorded in archives like ice cores, such profiles can be used as proxy to reconstruct paleo-temperature variations in arctic regions. However, a quantitative interpretation of these temperature reconstructions is a challenging task, since the water isotope composition depends on various climate components such as sea surface temperatures (SSTs) and circulation patterns, which are locally varying. Thus, to be able to analyze the impacts of each of these climate variables on the isotope ratios in ice cores, we enabled the regional climate model COSMO-CLM to consider water isotopes (CCLMiso), based on earlier work of Pfahl et al., (2012).

Within the BMBF funded project PalMod we use CCLMiso for a dynamical downscaling of isotope-enabled global Earth System Models (ESMs) and compare the results with proxies. In this way the capability of the models to reproduce paleo-climate conditions is assessed and the understanding of paleo-climate dynamics can potentially be improved. During PalMod, CCLMiso was successfully applied in climate simulations for Europe (Christner et al., 2018). By means of several 10 year time-slice simulations Christner et al., (2018) could show that the isotope ratios in precipitation strongly depend on evaporation processes below the cloud base.

In a next step, CCLMiso will be applied on paleo-climate simulations in the Arctic region (50km horizontal resolution, 159 x 176 x 50 grid points). The results of first present day test cases indicate that CCLMiso is able to simulate adequately the regional climate conditions in Greenland. The comparison of simulation results with proxies shows that CCLMiso better reflects the measured isotopic compositions in ice cores than coarse ESMs (Figure 22), and can therefore be used in arctic paleo-climate simulations. Of great interest in this context are the Last Glacial Maximum (LGM, ~ 20000 years ago) and the warm period in the Mid-Holocene (MH, ~ 8000 years ago), since both constitute special climatological situations whose formation processes are not fully understood. For this, the simulation periods need to be increased from 10 to 30 year time-slices to get robust climatological results. This leads to a computational demand of approximately 90000 node-hours for the next year.

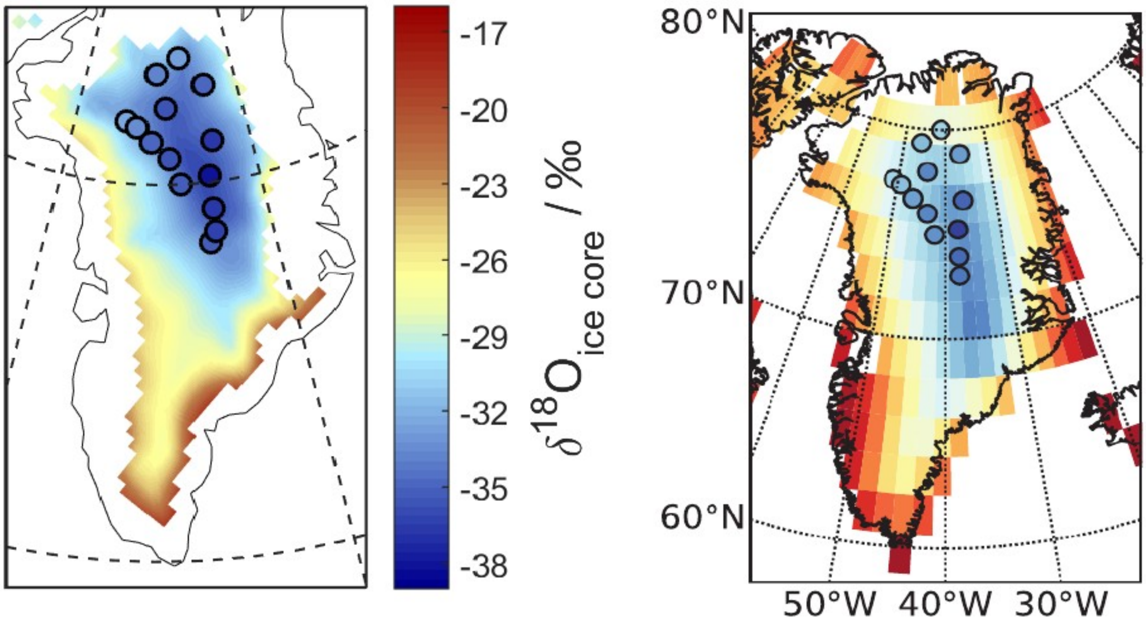

Fig. 22: Simulated annual δ18O composition for the period 2000-2014, for CCLMiso (left) and ECHAM6_wiso (right) in comparison to measured isotopic ratios in ice cores (colored rings).

References

Christner, E., Aemisegger, F., Pfahl, S., Werner, M., Cauquoin, A., Schneider, M., Hase, F., Barthlott, S., & Schädler, G. (2018). The Climatological Impacts of Continental Surface Evaporation, Rainout, and Subcloud Processes on δD of Water Vapor and Precipitation in Europe. Journal of Geophysical Research: Atmospheres, 123(8), 4390-4409.

S. Pfahl, H. Wernli, and K. Yoshimura. The isotopic composition of precipitation from a winter storm - a case study with the limited-area model COSMOiso. Atmospheric Chemistry and Physics, 12(3):1629–1648, feb 2012.

WP3.3 TP02 (FUB)

In WP-3.3 TP02 (FUB), the Data Assimilation (DA) of proxy data (pollen-based temperature reconstructions) is successfully tested. We have used the pre-computed Regional Climate Model simulations and an off-line DA approach and evaluated our set-up for the mid-Holocene time. Prior to application of the DA approach to mid-Holocene, we conducted a perfect model experiment using and ensemble of COSMO-CLM model simulations (5 members × 36 years and 8 × 10 years), which we conducted last year. However, after submitting the paper, we received 3 different reviews which demanded running a new set of ensembles with lagged initialization approach, as well as, testing new set-ups for DA. A complete representation of the results is available in our recently published paper in Climate of the Past, in which we acknowledged DKRZ:

Fallah, B., Russo, E., Acevedo, W., Mauri, A., Becker, N., and Cubasch, U.: Towards high-resolution climate reconstruction using an off-line data assimilation and COSMO-CLM 5.00 model, Clim. Past, 14, 1345-1360, https://doi.org/10.5194/cp-14-1345-2018, 2018.

Here, a brief abstract of the results:

"We design a computationally affordable DA to assimilate yearly pseudo-observations and real observations into an ensemble of COSMO-CLM high-resolution regional climate model

(RCM) simulations over Europe, for which the ensemble members slightly differ in boundary and initial conditions. Within a perfect model experiment, the performance of the applied DA scheme is evaluated with respect to its sensitivity to the noise levels of pseudo-observations. It was observed that the injected bias in the pseudo-observations linearly impacts the DA skill. Such experiments can serve as a tool for the selection of proxy records, which can potentially reduce the state estimation error when they are assimilated. Additionally, the sensitivity of COSMO-CLM to the boundary conditions is addressed. The geographical regions where the model exhibits high internal variability are identified. Two sets of experiments are conducted by averaging the observations over summer and winter. Furthermore, the effect of the spurious correlations within the observation space is studied and a optimal correlation radius, within which the observations are assumed to be correlated, is detected. Finally, the pollen-based reconstructed quantities at the mid-Holocene are assimilated into the RCM and the performance is evaluated against a test dataset. We conclude that the DA approach is a promising tool for creating high-resolution yearly analysis quantities. The affordable DA method can be applied to efficiently improve climate field reconstruction efforts by combining high-resolution paleoclimate simulations and the available proxy records."

Additionally, we started with the downscaling milestone of the project using the available CMIP5 MPI-ESM simulations at DKRZ for the Last Glacial Maximum and Mid-Holocene over Arctic and Europe regions. Prior to that, we tested the performance of the default model set-up for the CORDEX Arctic region forced by ERAInterim. The default set-up of the model has a warm bias over Greenland (Fig. 25a). Therefore, a set of sensitivity simulations where conducted to reduce the bias (16 simulations × 10 years). Finally, we were forced to reduce the time-step of the model to 150 seconds which increases the computational expenses.

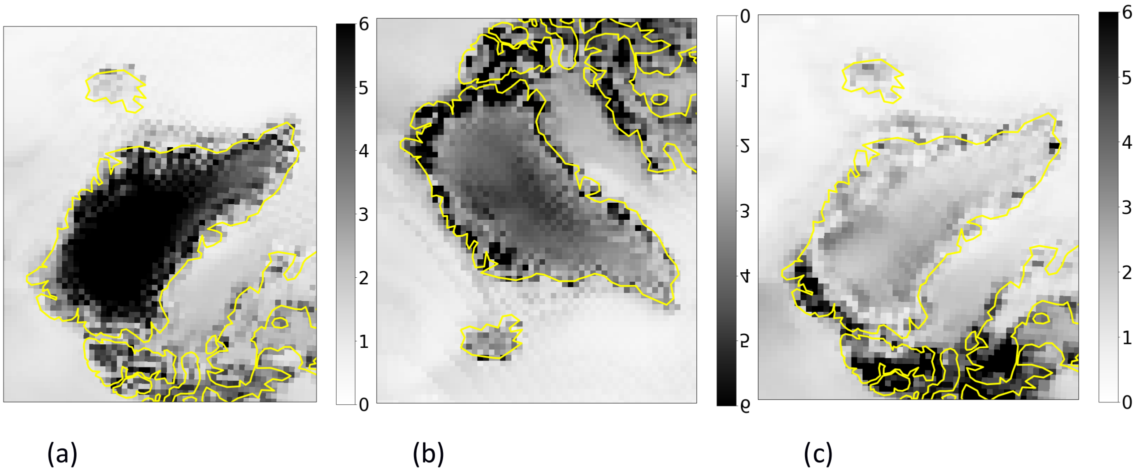

Fig. 23: RMSE (K) of monthly T2M for (a) un-tuned simulation and (b) tuned simulation against Modern-Era Retrospective analysis for Research and Applications, Version 2 (MERRA2) and (c) the differences of ERAInterim and MERRA2. The simulation are 10 years. Both reanalysis data are mapped on CCLM grid using the nearest neighbor.

Simulations are based on COSMO-CLM 5.00

- 21 × 10 years of CCLM simulations with off-line DA with time-lagged initialization.

- 100 years of CCLM simulations for mid-Holocene over Arctic (finished) with dt=150 sec..

- 100 years of CCLM simulations for LGM Arctic (will be finished till end of October) with dt=150 sec.

- 16 × 10 years of CCLM simulations driven by ERAInterim for tuning the model over Arctic region.

Resource utilization used till 15.10.2018 :

- Mistral computer time [node hours]: 10500
- Lustre work [GiB] : 1829
- HPSS arch [GiB] : 46647

Project: **993**

Project title: **PalMod WG4**

Project lead: **Hendryk Bockelmann**

Report period: **2018-01-01 to 2018-12-31**

Work Package 4.1

We continued our investigation of parameters in marine ecosystem models. For the systematic investigation of these parameters we implemented a framework for constrained optimization. The proposed optimization runs were started but are not finalized up to now. First results should be expected by the end of the year and will be reported in 2019 all together.

Work Package 4.2

The effect of time varying orography, land-sea mask and ocean bathymetry has been tested in a set of simulations with MPI-ESM-CR. Baseline simulation was a deglacial simulation using topographic and cryospheric forcing (ice sheets and net meltwater forcing) from the ICE-6G reconstruction. The adaptation of ocean bathymetry and land-sea-mask was performed using the automatic algorithm developed by Meccia and Mikolajewicz (under revision). The adaptation was performed every 10 years. In one sensitivity experiment starting from 21kyrBP the land-sea mask was kept constantly at 21 kyrBP values, but the ocean depth was adapted. In another sensitivity run the ocean bathymetry was also kept constant at 21 kyrBP values. Results are shown in Fig. 24. Results show, that the AMOC is seriously affected by keeping the land-sea mask constant. From approximately 13 kyr BP onward, when the deglaciation leads to massive changes in land-sea mask. The lack of the East Greenland Shelf in the sensitivity experiments makes the deepwater formation in the Nordic Seas more vulnerable to meltwater outflow from the Arctic. Thus the AMOC shows a strong oscillatory behaviour between and 13 and 7 kyrBP. After 7kyrBP the AMOC is still 3 Sv weaker than in the ICE-6G baseline run. The results show, that the changes in land-sea mask are more important than the changes in ocean bathymetry.

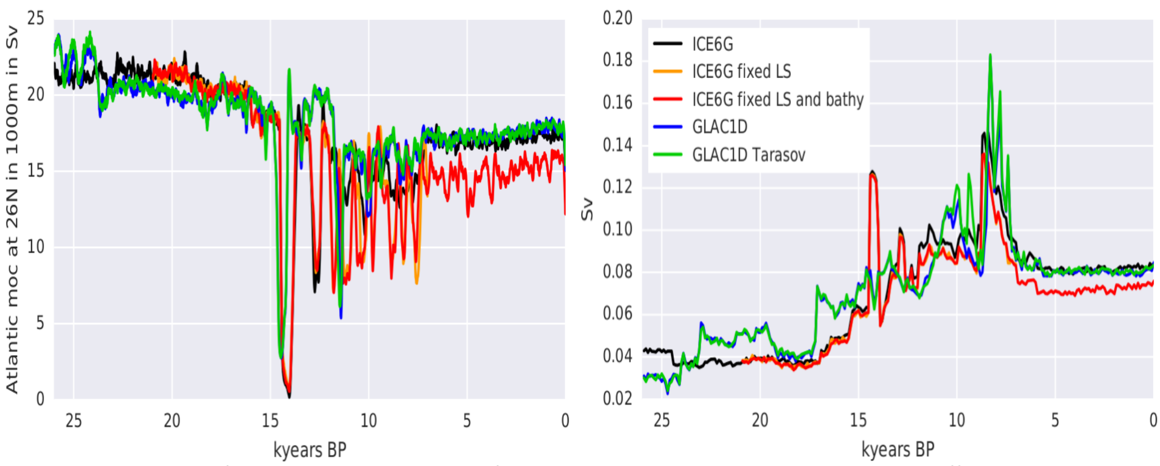

Fig. 24: Time series of AMOC at 26°N and net freshwater input into the Labrador Sea, Baffin Bay and Hudson Bay.

An automatic algorithm to calculate the topographic input parameters (e.g. runoff directions) was developed (Riddick et al. 2018). The effect of changes in dynamic river routing was tested in a series of time slice experiments with different run-off parameter sets derived with different methods including the standard hand-edited data set used in MPI-ESM. The final automatic procedure was tested against the algorithm developed by Lev Tarasov. Here a long deglacial simulation using the GLAC1D reconstruction from Tarasov was used as prescribed boundary condition using the MPI-ESM-CR with automatic adaptation of land-sea mask and ocean bathymetry using the Meccia and Mikolajewicz algorithm. Results show that both the Tarasov and our algorithm give very similar river routing directions. As an example the effective freshwater flux (rivers + precipitation – evaporation) into the Labrador Sea and the Hudson Bay are shown. Except for the period between 10 and 8.5 kyrBP, the net freshwater is almost identical (see Fig.24). Thus the resulting changes in AMOC are also very similar. The tests for the automatic adaptation algorithms for orography, land-sea-mask, ocean bathymetry and river routing was quite successful and we now have the ability to perform adequate long-term paleo simulations also for periods with strongly changing ice volume.

Publications

Riddick, T., Brovkin, V., Hagemann, S., and Mikolajewicz, U.: Dynamic hydrological discharge modelling for coupled climate model simulations of the last glacial cycle: the MPI-DynamicHD model version 3.0, Geosci. Model Dev., 11, 4291-4316, https://doi.org/10.5194/gmd-11-4291-2018, 2018.

Meccia, V. L. and U. Mikolajewicz () Interactive ocean bathymetry and coastlines for simulating the last deglaciation with the Max Planck Institute Earth System Model (MPI-ESM-v1.2), Geosci. Model Dev. Discuss., https://doi.org/10.5194/gmd-2018-129, in review, 2018.

Work Package 4.3

The planned application of parallel-in-time methods using two ECHAM/MPI-ESM resolutions needed to be postponed due to technical difficulties with the model code. These difficulties are not due to the parallel-in-time method itself, but to coupling and restart issues in the software. Therefore, only a negligible part of the compute time was used.

Work Package 4.4

TP1

To match the requirements of the working groups 1 and 2 regarding the runtime of the coupled MPI-ESM model , we extended the classical data parallelism (decomposition of the underlying mesh) by introducing additional task parallelism within the ECHAM6 atmospheric model. Profiling the execution time of the coupled MPI-ESM model at coarse and low resolution revealed that the most time consuming part in ECHAM6 is the radiative transfer. Hence, we extracted the source code that is used for radiation from the rest of the ECHAM6 code and enhanced the interprocess communication features to execute these parts in parallel.

In a first step we have shown that the remotely executed radiation, which still runs synchronously to the atmospheric model (basically the dynamical core and the remaining physics), does not impact the results and imposes only very little communication overhead in the order of less than 1% (Fig. 25 left). Finally, we executed the fully asynchronous scheme to get rid of the waiting times in each component (Fig. 25 right). Still there is room for improvements since the workload balance between the two components is currently not optimal. If the coupling back and forth is not aligned by a suitable choice of timesteps, either the radiation tasks or the atmospheric tasks wait for the other component. Also the YAXT based data exchange between the two process groups will be optimized further to e.g. allow for different decompositions. But already with this version the scalability of the ECHAM6 model in coarse resolution could be improved (Fig. 26).

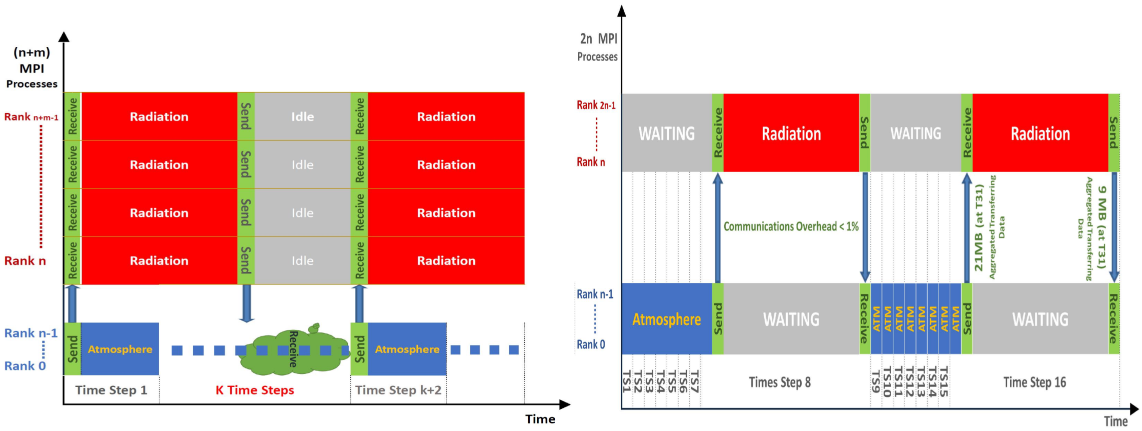

Fig. 25: Schematic execution of remote radiation in ECHAM6; synchronous mode for development purpose (left) and asynchronous mode (right).

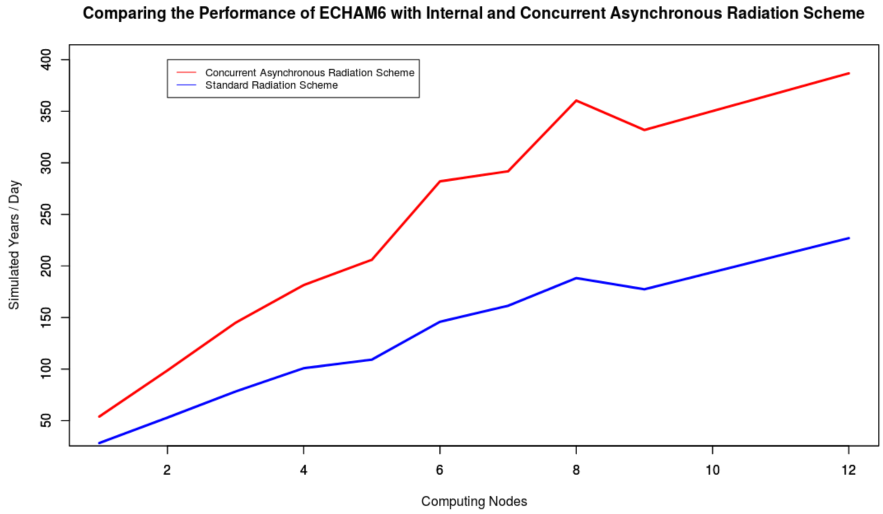

Fig. 26: Scaling behaviour of the ECHAM6 CR model. For the concurrent asynchronous radiation scheme the number of nodes is twice the amount noted on the x-axis.

TP3

The standard model MPI-ESM uses a static land-sea distribution. For climate simulations on glacial timescales, MPIOM has been adjusted to handle changes in ocean topography automatically in WP4.2. The aim of WP4.4 TP3 is to adjust the biogeochemical model HAMOCC to cope with these transiently changing coastlines being introduced in MPIOM. Therefore, a new model setup of HAMOCC has been developed in which the HAMOCC restart files are adjusted automatically to the changes in the land-sea mask as well as bottom topography. Biogeochemical state variables are redistributed horizontally and vertically, in the same manner in which the physical tracers salinity and temperature are treated in MPIOM. Mass of the marine biogeochemical tracers and variables is conserved – there is yet no carbon or nutrient exchange between land and ocean in this step. This has been thoroughly tested in ocean only (MPIOM/HAMOCC) runs.

In the second step, we have worked on the implementation of the coupling between land and ocean at the transiently changing land-sea interface. Fluxes of carbon and nutrients from land to the ocean which take place in case of the flooding of land grid cells are now accounted for. Terrestrial organic matter is stored in different pools such as biomass, litter and humus, which have to be distinguished with respect to composition and degradation properties. Thus, additional tracers in the water column and variables in the sediment have been introduced into HAMOCC to represent terrestrial organic matter in the ocean. This terrestrial organic matter differs in stoichiometry and remineralization time-scales from organic matter of oceanic origin. When being decomposed, carbon and nutrients contained in the terrestrial material become available for ocean biogeochemical cycling and can affect the uptake and storage of CO_2 in the ocean. The implementation has to be completed and needs to be thoroughly tested in transient simulations with the coupled model.

The model development and the ocean only test runs did not use much CPU time. The transient test runs with the coupled model will, however, start soon and will require substantially more computing time and storage space.

TP4

We proposed to integrate adaptive mesh refinement (AMR) into tracer transport module of ECHAM6. We expect an improvement of accuracy of the results of existing model with AMR in single component arise from the interaction of physical processes in the climate models. Ultimately, a data structure that is able to run on adaptive mesh will be used. In the meantime, the data structure is compatible with the existing model that can take the data from the host model to the AMR modules. We also modified the original tracer transport scheme in the ECHAM6 such that it is able to run on adaptive meshes. We tested our scheme with idealized test cases to make sure it shares similar numerical properties as the original scheme. Up to now, we managed to integrate our code into the ECHAM-HAMMOZ model without parallelisation, which allowed us to run several preliminary test experiments.